Equilibrium properties of transitionmetal ion–argon clusters via simulated annealing

Robert L. Asher, David A. Micha, and Philip J. Brucat

Citation: The Journal of Chemical Physics **96**, 7683 (1992); doi: 10.1063/1.462369
View online: http://dx.doi.org/10.1063/1.462369
View Table of Contents: http://scitation.aip.org/content/aip/journal/jcp/96/10?ver=pdfcov
Published by the AIP Publishing

Equilibrium properties of transition-metal ion–argon clusters via simulated annealing

Robert L. Asher, David A. Micha, and Philip J. Brucat
Quantum Theory Project and Department of Chemistry, University of Florida, Gainesville, Florida 32611

(Received 13 November 1991; accepted 7 February 1992)

The geometrical structures of $M^+(Ar)_n$ ions, with $n = 1$–14, have been studied by the minimization of a many-body potential surface with a simulated annealing procedure. The minimization method is justified for finite systems through the use of an information theory approach. It is carried out for eight potential-energy surfaces constructed with two- and three-body terms parametrized from experimental data and *ab initio* results. The potentials should be representative of clusters of argon atoms with first-row transition-metal monocations of varying size. The calculated geometries for $M^+ = Co^+$ and V^+ possess radial shells with small (ca. 4–8) first-shell coordination number. The inclusion of an ion-induced-dipole–ion-induced-dipole interaction between argon atoms raises the energy and generally lowers the symmetry of the cluster by promoting incomplete shell closure. Rotational constants as well as electric dipole and quadrupole moments are quoted for the $Co^+(Ar)_n$ and $V^+(Ar)_n$ predicted structures.

I. INTRODUCTION

Molecular systems which contain only weak interatomic forces, such as the forces in clusters of rare-gas atoms, serve as good models for ion solvation. Small clusters of a transition-metal-ion and rare-gas atoms provide simplified and tractable models for solvent interaction in the absence of thermal averaging and of complicating forces arising from permanent multipoles. These systems allow for detailed study of nontraditional "floppy" molecules and for the clarification of the meaning of their conformations.[1] The use of clusters or cluster ions as models for solvent interactions is not new.[2,3] Crossed-beam scattering[4] and photodissociation studies[5] provide the necessary pairwise potential-energy surfaces (PESs) required for accurate modeling. Clusters of recent experimental interest[6] include the general compounds $(M^+)L_n$ where M = V, Co, Ni, Cu, Zr,..., and L = He, Ne, Ar, Kr, N_2, H_2O, CO_2, N_2O,... . While the present study deals with only M = V and Co, and L = Ar for $n = 1$–14, similar treatments for the more complex clusters may be accomplished provided the PESs for these systems may be estimated.

Properties of the clusters Ar_n, $n = 4$–55, have been thoroughly studied using molecular-dynamics methods, and have been analyzed as examples of balanced structures.[7] These are structures predicted some time ago on mathematical grounds as resulting from particles on the surface of a sphere interacting with pairwise potentials.[8] Our studies refer to different clusters (with a central ion) and include three-atom potentials, but might also present some of the features of balanced structures. Here, however, we concentrate on the method of simulated annealing, and how atoms arrange on several shells (instead of just one) around each ion.

In this investigation, the global potential-energy minima and structures have been determined for the $(Co^+)Ar_n$ and $(V^+)Ar_n$ cluster ions using a Monte Carlo (MC) method of simulated annealing (SA). Since these systems contain many local minima, SA finds the global minimum by exploring the PES at random. The method of simulated annealing was first applied to atomic clusters by Wille;[9] more recently, Navon, Brown, and Robertson[10] applied the method to mixed rare-gas clusters.

The present study is a natural extension of the SA method to more complicated PESs involving transition-metal–rare-gas interactions. SA performs a biased random search, with the bias provided by a Boltzmann-type distribution that can be justified for a single finite system (our case) by means of an information theoretical approach. The introduction of a pseudotemperature in this approach leads to pseudothermodynamic properties. Equilibrium values such as moments of inertia and electric multipoles can be calculated during the minimization process. The global PES minima of these systems found by this procedure may then be used as a starting point for the molecular-dynamics modeling at finite temperature.

In what follows, the information theory approach is summarized in Sec. II. Section III gives the expressions required to calculate equilibrium moments of inertia, electric dipole and quadrupole moments from the derived global minimum conformations. Section IV details the construction of the many-atom potentials used in the simulation, which include two- and three-atom interaction terms. The simulated annealing procedure is summarized in Sec. V in the form of an algorithm which specifies the number of moves at each pseudotemperature, rejection criteria, and convergence tolerance. Extensive calculations with four different potentials for each ion, Co^+ and V^+, are presented in Sec. VI, emphasizing the effects of ion sizes and of induced-diple–induced-dipole forces on solvation shell conformations. The discussion in Sec. VII points out the qualitative features arising from the calculations, and prospects for fu-

ture applications of the same method to other properties and systems.

II. INFORMATION THEORETICAL APPROACH

We want to develop a treatment of SA similar to the one in thermodynamics but for our finite systems. This can be accomplished using concepts of information theory.[11] The Hamiltonian (H) for these clusters is taken to be the classical kinetic (K) plus potential (V) energy

$$H(\mathbf{p},\mathbf{q}) = K(\mathbf{p}) + V(\mathbf{q}), \tag{1}$$

where $\mathbf{p}$ is the set of momenta $\{\mathbf{p}_i\}$ in Cartesian coordinates for all atoms i, and $\mathbf{q}$ is the set of Cartesian coordinates $\{\mathbf{q}_i\}$. The standard definition of missing information, I,

$$I = -k\int d\mathbf{p}\, d\mathbf{q}\, P(\mathbf{p},\mathbf{q}) \ln P(\mathbf{p},\mathbf{q}), \tag{2}$$

where k is a dimensionality constant and $P(\mathbf{p},\mathbf{q})$ is the probability that the system will be in state $(\mathbf{p},\mathbf{q})$, is employed to describe a cluster or system of particles. I is maximized subject to the following constraints:

$$k\int d\mathbf{p}\, d\mathbf{q}\, P(\mathbf{p},\mathbf{q}) = 1, \tag{3}$$

$$k\int d\mathbf{p}\, d\mathbf{q}\, P(\mathbf{p},\mathbf{q}) R^{(\alpha)}(\mathbf{p},\mathbf{q}) = \langle R^{(\alpha)}(\mathbf{p},\mathbf{q})\rangle \tag{4}$$

with $R^{(\alpha)}(\mathbf{p},\mathbf{q})$ being some property of the system. Introducing the Lagrangian multipliers κ and λ_α, we require

$$\begin{aligned} I'[P(\mathbf{p},\mathbf{q}),\kappa,\lambda_\alpha] = &-k\int d\mathbf{p}\, d\mathbf{q}\, P(\mathbf{p},\mathbf{q}) \ln P(\mathbf{p},\mathbf{q}) \\ &+ \kappa(\kappa+1)k\int d\mathbf{p}\, d\mathbf{q}\, P(\mathbf{p},\mathbf{q}) \\ &+ \sum_\alpha \lambda_\alpha k\int d\mathbf{p}\, d\mathbf{q}\, P(\mathbf{p},\mathbf{q}) R_j^{(\alpha)} = \max, \end{aligned} \tag{5}$$

and therefore for all $(\mathbf{p},\mathbf{q})$

$$\frac{\partial I'}{\partial \kappa} = \frac{\partial I'}{\partial \lambda_\alpha} = \frac{\delta I'}{\delta P(\mathbf{p},\mathbf{q})} = 0. \tag{6}$$

In the canonical ensemble $\lambda_1 = \beta$ (the pseudoinverse temperature) and $R^{(1)}(\mathbf{p},\mathbf{q}) = H(\mathbf{p},\mathbf{q})$ so that

$$\kappa = -\ln\left(k\int d\mathbf{p}\, d\mathbf{q}\, e^{-\beta H(\mathbf{p},\mathbf{q})}\right) = -\ln\Omega, \tag{7}$$

where Ω is the partition function. The probability is now

$$P(\mathbf{p},\mathbf{q}) = e^{\kappa - \beta H(\mathbf{p},\mathbf{q})}. \tag{8}$$

The pseudointernal energy of the cluster will be given by

$$\frac{\partial \kappa}{\partial \beta} = -\frac{\partial \ln\Omega}{\partial \beta} = \langle H(\mathbf{p},\mathbf{q})\rangle = U, \tag{9}$$

while the average value of any property R of the system is given by

$$\langle R\rangle = \int d\mathbf{p}\, d\mathbf{q}\, e^{-\beta H(\mathbf{p},\mathbf{q})} R(\mathbf{p},\mathbf{q}) \Big/ \int d\mathbf{p}\, d\mathbf{q}\, e^{-\beta H(\mathbf{p},\mathbf{q})}. \tag{10}$$

In particular, the average value of the potential energy is just

$$\langle V\rangle = \int d\mathbf{q}\, e^{-\beta V(\mathbf{q})} V(\mathbf{q}) \Big/ \int d\mathbf{q}\, e^{-\beta V(\mathbf{q})}, \tag{11}$$

since V is not a function of $\mathbf{p}$. The average kinetic energy with respect to a space-fixed reference frame is a function of the pseudoinverse temperature given by

$$\langle K\rangle = \frac{3N}{2\beta}, \tag{12}$$

and the pseudointernal energy will be the sum of the two averages or just the average of the Hamiltonian, $U = \langle K\rangle + \langle V\rangle = \langle H\rangle$.

A pseudoheat capacity of the system may be defined as

$$C = \beta^2 \frac{\partial^2 \kappa}{\partial^2 \beta}, \tag{13}$$

which yields a simple expression

$$C = \beta^2(\langle H\rangle^2 - \langle H^2\rangle). \tag{14}$$

Now as $\beta\to\infty$, or as the pseudotemperature goes to zero, we have $|\langle K^2\rangle| \ll |\langle V^2\rangle|$ and $|\langle K\rangle| \ll |\langle V\rangle|$. This means that the internal energy approaches the equilibrium potential energy $U \approx V_{eq}$ and that the heat capacity goes to zero, $C \approx 0$.

III. CALCULATION OF EQUILIBRIUM PROPERTIES

Equilibrium properties can be obtained for $\beta\to\infty$, that is, for a pseudotemperature of 0.0 K. For this β, we can immediately go about calculating the moment of inertia, dipole moment, and quadrupole moment of the clusters at their potential-energy global minimum. The components of the moment of inertia tensor are simply

$$\begin{aligned} (\mathbf{I})_{\xi\eta} = &\, m_+[\delta_{\xi\eta}(\mathbf{r}_+)^2 - (\mathbf{r}_+)_\xi(\mathbf{r}_+)_\eta] \\ &+ \sum_{i=1}^{n} m_i[\delta_{\xi\eta}(\mathbf{r}_i)^2 - (\mathbf{r}_i)_\xi(\mathbf{r}_i)_\eta], \end{aligned} \tag{15}$$

where we use $\mathbf{r}_i$ and $\mathbf{r}_+$ to indicate positions of Ar atoms and the metal ion in center-of-mass coordinates, with $\xi,\eta = x,y,z$ components of these vectors and $r^2 = x^2 + y^2 + z^2$ (see, for example, Marion[12]).

The dipole moment of the cluster can be calculated in the center-of-charge (COC) coordinates by the sum of all of the induced dipoles (see, for example, Ref. 13)

$$\mathbf{D}^{\mathrm{COC}} = \alpha q_+ \sum_{i=1}^{n} \frac{\mathbf{R}_i}{R_i^3}, \tag{16}$$

where R_i is the distance from the ith Ar atom to the ion, α is the polarizability of the Ar, and q_+ is the charge on the ion. Alternatively, the dipole moment in center-of-mass (COM) coordinates can be given as

$$\mathbf{D}^{\mathrm{COM}} = \sum_{i=1}^{n} q_i^- \mathbf{r}_i^- + \sum_{i=1}^{n} q_i^+ \mathbf{r}_i^+ + q_+ \mathbf{r}_+, \tag{17}$$

where

$$q_i^{\pm} \equiv \pm \frac{\alpha q_+}{2r_{\mathrm{Ar}} R_i^2} \tag{18}$$

are charges induced at the Ar and $2r_{\mathrm{Ar}}$ is the distance between fictitious charges in the induced dipole. The distances to the charges of the induced dipole are given by

$$\mathbf{r}_i^{\pm} = \mathbf{r}_i \pm \frac{r_{\mathrm{Ar}} \mathbf{R}_i}{R_i}. \tag{19}$$

The COM dipole moment reduces to a simple form

$$\mathbf{D}^{\mathrm{COM}} = q_+ \left(\mathbf{r}_+ + \alpha \sum_{i=1}^{n} \frac{\mathbf{R}_i}{R_i^3} \right), \tag{20}$$

which is the COC dipole plus the displacement of the ion from the COM of the cluster.

The COC quadrupole moment tensor is given by

$$\mathbf{Q}_{\xi\eta}^{\mathrm{COC}} = \sum_{i=1}^{n} q_i^+ \left[3(\mathbf{R}_i^+)_\xi (\mathbf{R}_i^+)_\eta - (R_i^+)^2 \delta_{\xi\eta} \right] + \sum_{i=1}^{n} q_i^- \left[3(\mathbf{R}_i^-)_\xi (\mathbf{R}_i^-)_\eta - (R_i^-)^2 \delta_{\xi\eta} \right], \tag{21}$$

where

$$\mathbf{R}_i^{\pm} = \mathbf{R}_i \left(1 \pm \frac{r_{\mathrm{Ar}}}{R_i} \right) \tag{22}$$

are the positions of the charges of the induced dipoles. The COM quadrupole moment can be derived from

$$\mathbf{Q}_{\xi\eta}^{\mathrm{COM}} = q_+ \left[3(\mathbf{r}_+)_\xi (\mathbf{r}_+)_\eta - (r_+)^2 \delta_{\xi\eta} \right] + \sum_{i=1}^{n} q_i^+ \left[3(\mathbf{r}_i^+)_\xi (\mathbf{r}_i^+)_\eta - (r_i^+)^2 \delta_{\xi\eta} \right] + \sum_{i=1}^{n} q_i^- \left[3(\mathbf{r}_i^-)_\xi (\mathbf{r}_i^-)_\eta - (r_i^-)^2 \delta_{\xi\eta} \right] \tag{23}$$

and from Eqs. (18) and (19) leading to

$$\mathbf{Q}_{\xi\eta}^{\mathrm{COM}} = q_+ \left[3(\mathbf{r}_+)_\xi (\mathbf{r}_+)_\eta - (\mathbf{r}_+)^2 \delta_{\xi\eta} \right] + \frac{\alpha q_+}{2r_{\mathrm{Ar}}} \sum_{i=1}^{n} \left\{ 3 \left[\left(\mathbf{r}_i + \frac{r_{\mathrm{Ar}} \mathbf{R}_i}{R_i} \right)_\xi \left(\mathbf{r}_i + \frac{r_{\mathrm{Ar}} \mathbf{R}_i}{R_i} \right)_\eta - \left[\left(\mathbf{r}_i - \frac{r_{\mathrm{Ar}} \mathbf{R}_i}{R_i} \right)_\xi \left(\mathbf{r}_i - \frac{r_{\mathrm{Ar}} \mathbf{R}_i}{R_i} \right)_\eta \right] - \left\{ 4 r_{\mathrm{Ar}} \left(\frac{\mathbf{r}_i \cdot \mathbf{R}_i}{R_i} \right) \delta_{\xi\eta} \right\} \Big/ R_i^2 \right] \right\}, \tag{24}$$

which simplifies to give

$$\mathbf{Q}_{\xi\eta}^{\mathrm{COM}} = q_+ \left(3(\mathbf{r}_+)_\xi (\mathbf{r}_+)_\eta - r_+^2 \delta_{\xi\eta} \right) + \alpha q_+ \sum_{i=1}^{n} \left(\left\{ 3 \left[(\mathbf{r}_i)_\xi \left(\frac{\mathbf{R}_i}{R_i} \right)_\eta + (\mathbf{r}_i)_\eta \left(\frac{\mathbf{R}_i}{R_i} \right)_\xi \right] - 2\delta_{\xi\eta} \left(\frac{\mathbf{r}_i \cdot \mathbf{R}_i}{R_i} \right) \right\} \Big/ R_i^2 \right). \tag{25}$$

The arbitrary coordinate system chosen at the start of the calculation is transformed by rotation into the principal moment of inertia frame. In this frame, the moment of inertia tensor is diagonal with three unique elements I_a, I_b, and I_c which are related to the rotational constants A, B, and C by $A = h/8\pi^2 c I_a$, etc., where h and c are Planck's constant and the speed of light, respectively, and $I_a \leqslant I_b \leqslant I_c$ as is the usual ordering (see Ref. 14). The COM electric dipole and

TABLE I. Potential parameters for (M^+)–Ar, Ar–Ar and dipole–dipole interactions. Potentials (i) and (iii) are for Co^+; (ii) and (iv) for V^+.

Metal–rare-gas interaction parameters

Potential	D_e (eV)	D_M (eV)	R_e (Å)	ω_e (cm^{-1})	R_s (Å)	a ($Å^{-1}$)	a_s ($Å^{-1}$)	From Ref.[a]
i	0.524	0.5104	1.84	238	2.76	1.978	3.956	5
ii	0.381	0.3708	1.99	193	2.98	1.820	3.640	5
iii	0.403	0.4032	2.43	177	3.909	1.840	3.680	13
iv	0.299	0.2992	2.64	143	4.364	1.679	3.358	13

Argon–argon interaction parameters[b]

C_6^*	−1.180	b_0	−0.7
C_8^*	−0.611 8	b_1	1.8337
C_{10}^*	0	b_2	−4.5740
x_0	1.126 3	b_3	4.3667
x_1	1.400	γ	6.279
D_e	0.012 07 eV	R_e	3.760 Å

Dipole–dipole interaction parameters

R_c (Å)	b_c ($Å^{-1}$)	α_{Ar} ($Å^3$)
2.00	10.0	1.66

[a] D_e, R_e, and ω_e were taken from Refs. 5 and 13, the additional parameters were obtained from a fit to these three values using the MS4 potential.

[b] All parameters taken from Ref. 4.

quadrupole moments are also calculated in this frame.

The moment of inertia tensor is symmetric and is easily diagonalized by a rotation from the space-fixed reference frame to the body-fixed reference frame, to obtain the principal moments of inertia. The dipole vectors and quadrupole tensors can similarly be transformed to the principal moments frame.

IV. CONSTRUCTION OF THE MANY-ATOM POTENTIAL

The total potential energy for a $(M^+)L_n$ cluster is assumed to be a sum of two-atom and three-atom interactions,

$$V=\sum_{1<i<n} V_{M^+L_i}+\sum_{1<i<j<n} V_{L_iL_j}+\sum_{1<i<j<n} V_{M^+L_iL_j}. \tag{26}$$

The first term is the potential due to the charged metal ion interacting with the rare gas L_i. The second, two-atom, term is the interaction of two rare-gas atoms L_i and L_j, and the three-atom term contains the interaction of the rare-gas atomic dipoles induced by the metal ion. Other interactions in the multipole expansion have not been included but are assumed to be small in comparison with the terms above.

A. The M^+–L potential

The properties of first-row transition-metal ions complexed to a single Ar atom have been investigated previously both experimentally[5] and by *ab initio* theory.[15] Experimental results confirm the behavior of the long-range potential as $1/R^4$ and provide very accurate well depths, D_e, for the ground-state surface. Theory has provided dissociation energies, vibrational frequencies, ω_e, and equilibrium internuclear distances, R_e, for the ground state. Theory systematically underestimates the dissociation energy of the molecules by ca. 20%. Experimenters[5] have estimated ω_e and R_e for ground states by inference from excited-state properties. Again, theory systematically overestimates equilibrium bond lengths and underestimates vibrational frequencies. We have chosen four sets of parameters for $\{D_e,R_e,\omega_e\}$ that are presently available from the experimenters' and theorists' determinations of the properties of $CoAr^+$ and VAr^+. These parameters are listed in Table I, for potentials labeled (i), (ii), (iii), and (iv), chosen in order of increasing ionic radii. Potentials (i) and (ii) are our parametrized expressions from experiments for Co^+ and V^+, while (iii) and (iv) are our parametrized expressions from theory for Co^+ and V^+, respectively.

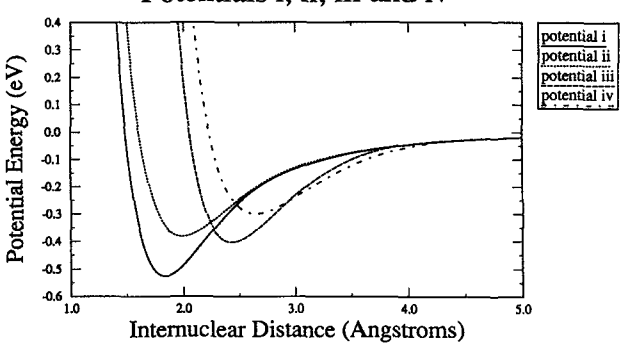

FIG. 1. Plot of the various parametrizations of the MS4 potential. (i) and (ii) represent experimental parameters for Co^+–Ar and V^+–Ar respectively. (iii) and (iv) are the MS4 with theoretical parameters for Co^+–Ar and V^+–Ar, respectively.

We have chosen to fit a modified Morse potential to the above $\{D_e,R_e,\omega_e\}$ parameters. This potential has the form

$$V_{M^+L}(R)=[1-f_s(R)]V_M(R)+f_s(R)V_4(R), \tag{27}$$

where V_M is the usual Morse potential

$$V_M(R)=D_M[e^{-2a(R-R_e)}-2e^{-a(R-R_e)}], \tag{28}$$

and V_4 is the charge-induced dipole potential

$$V_4(R)=\frac{-\alpha q^2}{2R^4}. \tag{29}$$

The asymtotic form of this potential is given by the literature value[16] of the polarizability of Ar, $\alpha=1.66$ Å^3. The switching function $f_s(R)$ between the Morse potential and the long-range asymptotic form was chosen as

$$f_s(R)=[1+e^{-a_s(R-R_s)}]^{-1}, \tag{30}$$

where R_s is the point at which switching is done and a_s determines the range of the switching. The values of the constants in Eqs. (28) and (30) chosen to fit $\{D_e,R_e,\omega_e\}$ are also found in Table I. We refer to this as the Morse-switch-4 (MS4) potential. The various parametrizations for the MS4 potentials (i)–(iv) are displayed graphically in Fig. 1.

B. The Ar–Ar potential

The crossed-beam studies by Parson, Lee, and Siska[4] have given the Ar–Ar potential, broken into three regions, as a Morse potential joined to the long-range van der Waals interaction by a spline function,

$$V^*(R^*)=\begin{cases} e^{-2\gamma(R^*-1)}-2e^{-\gamma(R^*-1)}, & R^*<x_0, \\ b_0+(R^*-x_0)\{b_1+(R^*-x_1)\}[b_2+(R^*-x_1)b_3], & x_0<R^*\leqslant x_1, \\ \dfrac{C_6^*}{R^{*6}}-\dfrac{C_8^*}{R^{*8}}-\dfrac{C_{10}^*}{R^{*10}}, & x_1<R^*, \end{cases} \tag{31}$$

where the reduced coordinates are given by

$$R^*=R/R_e,$$
$$V^*(R^*)=V(R^*)/D_e,$$
$$C_n^*=C_n/(D_eR_e^n). \tag{32}$$

The constants for what they call the MSVIII potential are also included in Table I.

C. Interaction of charge-induced dipoles

The potential for the interaction of two charge-induced

dipoles,[13] a three-atom potential, is given by

$$V_{M^+L_iL_j}(\mathbf{R}_i,\mathbf{R}_j) = \frac{q_+^2\,\alpha_i\alpha_j}{(RR_iR_j)^3}\left\{(\mathbf{R}_i\cdot\mathbf{R}_j) - \frac{3(\mathbf{R}_i\cdot\mathbf{R})(\mathbf{R}_j\cdot\mathbf{R})}{R^2}\right\} f_c(R), \tag{33}$$

where R_i is the magnitude of the vector from the ion to L_i, R is the magnitude of the vector between L_i and L_j, α_i is the polarizability of L_i, and q_+ is the charge of the metal ion M^+. The potential is cut off at short distances to avoid unrealistic behavior, with the function

$$f_c(R) = (1 + e^{-b_c(R-R_c)})^{-1}, \tag{34}$$

where R_c is the cutoff distance and b_c governs the width of the cutoff.

We have found that this cutoff function must be very carefully chosen to avoid cutting off the potential at what would be typical Ar–Ar distances in the clusters. R_c and b_c were varied systematically to ensure that no equilibrium properties or structures were affected by their values. The cutoff is rapid and occurs at a considerably smaller distance than typical Ar–Ar separations in these cluster ions. See Table I, for chosen values of R_c and b_c.

V. SIMULATED ANNEALING PROCEDURE

A. General outline

Simulated annealing is a very convenient method for determining a global minimum on a surface with many local minima. Kirkpatrick, Gelatt, and Vecchi[17] first applied this method to discrete combinatorial optimization problems. Vanderbilt and Louie[18] extended this method to problems with continuous variables. The SA method is simply an extension of the Metropolis[19] Monte-Carlo algorithm.

Consider a function $V(\mathbf{q})$ to be minimized for $\mathbf{q} = (q_1,q_2,\ldots,q_n)$ defined in an n-dimensional space. The Metropolis Monte Carlo algorithm starts by choosing an initial conformation $\mathbf{q}_0$ and then makes random moves $\Delta\mathbf{q}_i$. After each step, ΔV is calculated from $V(\mathbf{q}+\Delta\mathbf{q}) - V(\mathbf{q})$. If ΔV is negative (the potential has been lowered) the step is accepted; otherwise, it is accepted with some probability $\exp[-\beta(\Delta V)]$. The step size $\Delta\mathbf{q}$ is chosen such that the ratio of accepted steps to rejected steps is about 50%. If the annealing, done by raising β, is carried out slowly, the system will avoid being trapped in shallow local minima. The pseudotemperature controls the values of V that are acceptable. Lowering β allows the system to jump among local minima; raising β forces it to remain at a low minimum. This change of β represents an annealing process and this process must be repeated several times to assure that the global minimum has been found.

B. Computational algorithm for simulated annealing

The procedure is implemented with the following algorithm.

1. Start with an initial inverse pseudotemperature β, a random initial conformation $\mathbf{q}$, and choose an initial magnitude $\Delta\mathbf{q}$ for atom displacement (step size).
2. Calculate the potential energy for $\mathbf{q}$, $V(\mathbf{q})$.
3. Choose a new configuration $\mathbf{q}' = \mathbf{q} + \Delta\mathbf{q}$ by displacing one atom at a time and calculate the new potential energy of the system $V(\mathbf{q}')$.
4. Calculate $\Delta V = V(\mathbf{q}') - V(\mathbf{q})$.
5. If $\Delta V < 0$ always accept the new configuration.
6. If $\Delta V > 0$ and $\exp(-\beta\Delta V)$ is smaller than a random number between 0 and 1, then accept the new configuration even though it is higher in energy; otherwise, reject it.
7. If the number of acceptances surpasses 50%, decrease the step size.
8. If the number of configuration changes reaches 1000, increase β.
9. Repeat steps 3 through 8 and continue until β has reached a β_{max} or until ΔV stays smaller than some tolerance τ.
10. Repeat the entire process to ensure that the global minimum has been located.

Step 3 is somewhat arbitrary. One could also move all the atoms at random, or in groups if one wishes to maintain certain symmetries.

VI. RESULTS

The minimum potential-energy configurations of $M^+(Ar)_n$ cluster ions, for $n = 1$–14, have been determined for eight different parametrizations of the many-body potential. Results can be discussed for a fixed number of Ar atoms while varying the type of potential, or for a given potential with an increasing number of Ar atoms. Tables II and III can be read as a matrix of results where potentials are varied along rows, and the number of Ar atoms is varied along columns.

Calculations labeled I–IV are based upon the M^+–Ar potential parameters labeled (i)–(iv) in Table I, the Ar–Ar potential (also from Table I), and no three- or higher-body terms. Conformations derived from those calculations are shown in Table II. The next four calculations are analogous but include the interaction of ion-induced-dipole forces discussed in Sec. IV C and are labeled I + dd through IV + dd. Corresponding conformations are shown in Table III. The potential parameters and calculations are numbered to correspond to metal ions of increasing size, thus the results along rows may also be interpreted to represent typical complexes of first-row transition-metal monatomic cations of increasing sizes from left to right.

A. Equilibrium conformations

Tables II and III show the equilibrium geometries and point-group symmetries for calculations I through IV and I + dd through IV + dd, respectively. For a given potential, increasing the number of atoms n leads to the formation of solvation shells. These are made up of atoms located at the same distance from the central ion, or within a narrow range of distances. As n is increased the innermost solvation shell

TABLE II. Conformations and point-group symmetries for $(M^+)Ar_n$ with many-atom potentials I–IV, constructed from M^+–Ar interactions (i)–(iv), the MSVIII Ar–Ar interaction (Ref. 4) and no three-body interaction.

	Conformations and point groups for $(M^+)Ar_n$			
n	I	II	III	IV
1	Linear $C_{\infty v}$	Linear $C_{\infty v}$	Linear $C_{\infty v}$	Linear $C_{\infty v}$
2	Linear $D_{\infty h}$	Bent C_{2v}	Bent C_{2v}	Bent C_{2v}
3	Trigonal planar D_{3h}	Trigonal planar D_{3h}	Pyramidal C_{3v}	Pyramidal C_{3v}
4	Tetrahedral T_d	Tetrahedral T_d	Tetrahedral T_d	Seesaw C_{2v}
5	ctet C_{3v}	ctet C_{3v}	Square pyramidal C_{4v}	Square pyramidal C_{4v}
6	ctet C_{2v}	Octahedral O_h	Octahedral O_h	Octahedral O_h
7	ctet C_{3v}	coct C_{3v}	coct C_{3v}	7-coordinate C_{2v}
8	ctet T_d	coct C_{2v}	Square antiprism S_8	Square antiprism S_8
9	ctet	coct	csap C_{4v}	csap C_{4v}
10	ctet	coct	csap S_8	csap S_8
11	ctet	ctet	csap C_{2v}	csap C_{2v}
12	ctet	ctet	csap	csap
13	ctet	ctet C_{3v}	csap	csap
14	ctet	ctet T_d	csap	csap

forms a core of argons strongly bound to the ion. Additional solvation atoms may simply cap faces of this shell, slightly distort it, or may even open it up and increase the coordination of the central ion with the Ar atoms of this innermost shell. It has been observed that this core of solvation atoms often has high symmetry or only slight distortions from high symmetry, thus, in these tables the labels of the clusters are based upon the symmetry of the innermost or first solvation shell. Structures with tetrahedral or near tetrahedral first shells are labeled ctet, for "capped tetrahedra." Structures with octahedral or near octahedral first shells are labeled coct. Structures with square antiprismatic first shells are labeled csap.

Figure 2 contains stick figures of some of the highly symmetric clusters which may form around the three mentioned core structures. Figure 2(a) is a symmetric $(M^+)Ar_{14}$ capped tetrahedral structure. This structure has a tetrahedral core, another tetrahedral shell capping the faces of the first shell, and then an octahedral third shell capping the edges of the second shell. The sticks joining atomic spheres have been drawn to describe the shapes of the solvation shells, and do not of course signify bonding of the Ar atoms. Figure 2(b) is a symmetric $(M^+)Ar_{14}$ capped octahedral structure. This structure has an octahedral core and then a cube capping that. Figure 2(c) is a $(M^+)Ar_8$ square antiprism structure. Symmetric capping of this structure can occur if two atoms go on the square faces and then four atoms go on triangular faces, giving an elongated octahedral second shell. As will be discussed later, these symmetric outer shells are not always the structures with a global potential minimum.

Looking at Table II for potential I, as we increase the number of argon atoms, we see the buildup of the first solvation shell, which is complete at $n = 4$. After the fourth Ar is

TABLE III. Conformations and point-group symmetries for $(M^+)Ar_n$ with many-atom potentials I–IV plus the (dd) potential of the charge-induced dipoles appearing in the three-body interaction.

	Conformation and point groups for $(M^+)Ar_n$ with three-body term			
n	I + dd	II + dd	III + dd	IV + dd
1	Linear $C_{\infty v}$	Linear $C_{\infty v}$	Linear $C_{\infty v}$	Linear $C_{\infty v}$
2	Linear $D_{\infty h}$	Linear $D_{\infty h}$	Linear $D_{\infty h}$	Linear $D_{\infty h}$
3	Trigonal planar D_{3h}	Trigonal planar D_{3h}	Trigonal planar D_{3h}	T-shaped C_{2v}
4	Tetrahedral T_d	Tetrahedral T_d	Tetrahedral T_d	Distorted tet C_{2v}
5	ctet C_{3v}	ctet C_{3v}	Square pyramidal C_{4v}	Square pyramidal C_{4v}
6	ctet C_{2v}	ctet C_{2v}	Octahedral O_h	Octahedral O_h
7	ctet	ctet C_{3v}	coct C_{3v}	7 coordinate
8	ctet	ctet	coct C_{2v}	Square antiprism S_8
9	ctet	ctet	coct C_s	csap C_{4v}
10	ctet	ctet	coct	csap
11	ctet	ctet	coct	csap
12	ctet	ctet	coct	csap
13	ctet	ctet	coct	csap
14	ctet	ctet	coct	csap

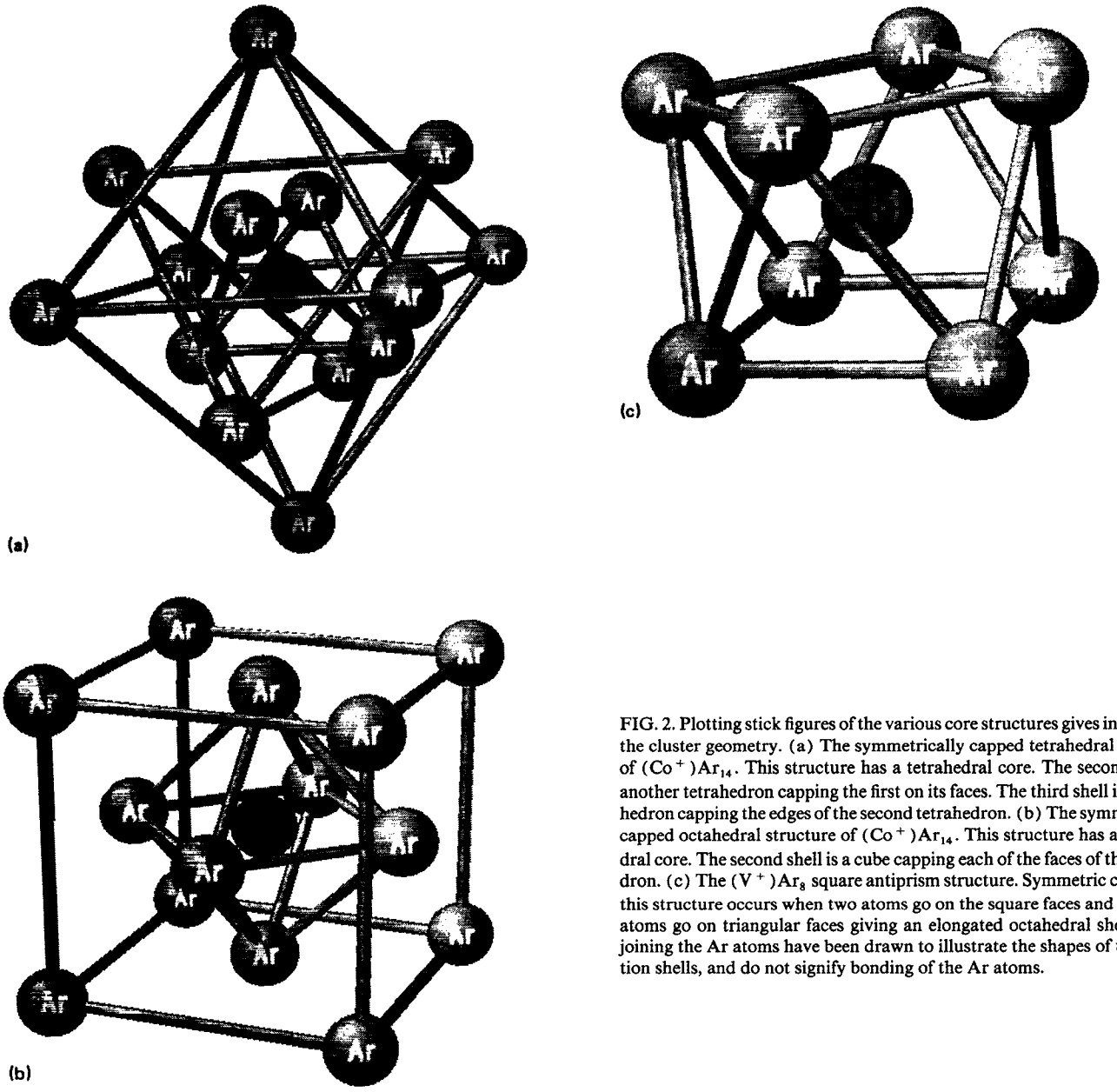

FIG. 2. Plotting stick figures of the various core structures gives insight into the cluster geometry. (a) The symmetrically capped tetrahedral structure of $(Co^+)Ar_{14}$. This structure has a tetrahedral core. The second shell is another tetrahedron capping the first on its faces. The third shell is an octahedron capping the edges of the second tetrahedron. (b) The symmetrically capped octahedral structure of $(Co^+)Ar_{14}$. This structure has an octahedral core. The second shell is a cube capping each of the faces of the octahedron. (c) The $(V^+)Ar_8$ square antiprism structure. Symmetric capping of this structure occurs when two atoms go on the square faces and then four atoms go on triangular faces giving an elongated octahedral shell. Sticks joining the Ar atoms have been drawn to illustrate the shapes of the solvation shells, and do not signify bonding of the Ar atoms.

added, additional argons cap the faces of the tetrahedron. This is continued until $n = 8$, at which point another tetrahedron has been formed. Argons 9–14 cap this second tetrahedron. If we take potential II as another example, we see similar behavior up to $n = 5$, for which we find a capped tetrahedral structure. However, at $n = 6$ we now see that the tetrahedral core is reformed into an octahedral shell. For this potential the tetrahedral core structure is a local minimum while the octahedral is the global minimum structure. As additional atoms go on, atoms 7–10 cap the octahedral core. At $n = 11$ we observe that the tetrahedral innermost shell now returns as the one with the global minimum and continues to prevail until at least $n = 14$. The binding energies of the capped tetrahedral and the capped octahedral structures are nearly the same for potential II.

Comparison of the various structures shows that potentials I and II make similar structures for $n = 1$, 3–5, and $n \geqslant 11$. An important difference between potentials I and II are the linear and bent conformations of $(M^+)Ar_2$ for the two potentials, respectively. The smaller equilibrium radius of potential I pulls the argons in so close to each other that their repulsion becomes more important than their attraction.

Using potential III and increasing n we find an array of symmetric structures which form the first solvation shell until $n = 7$, where a capping atom is placed on an octahedron. When the eighth Ar is added, however, the octahedral shell is lost and a square antiprism is formed. This remains as the innermost solvation shell for the remainder of the calculations. Potential IV gives similar structures with two glar-

TABLE IV. Shell properties for the various core structures.

Core structure	Shell number	Shell geometry	Shell radius (Å)	Maximum occupation
	Core and shell information for various ion sizes			
Tetrahedral	1	Tetrahedral	1.97–2.22	4
	2	Tetrahedral	3.65–3.83	4
	3	Octahedral	4.30–4.51	6
Octahedral	1	Octahedral	2.47–2.71	6
	2	Cubic	4.39–5.10	8
Square antiprism	1	Square antiprism	2.64–2.85	8
	2	Distorted octahedral	4.22–5.20	6

ing differences: a lower-symmetry "seesaw" structure appears at $n = 4$, and another low-symmetry seven-coordinate structure appears at $n = 7$. Both of these variations demonstrate that coordination with four or six argons is less favorable for the larger equilibrium distance of potential (iv).

Comparison between potentials while keeping n constant gives insight into the role of the size of the ion being solvated. For $n = 2$ we find that all potentials give a bent M^+Ar_2 with the exception of potential I for a very small ion. Potential I leads to a tetrahedral core for large n, while potential II leads to either octahedral or tetrahedral cores. Calculations for potentials III and IV, representing much larger ions, give larger square antiprism cores. The atoms of the core for potentials III and IV have slightly lower binding energy per argon than seen for I and II. The larger ions have more Ar atoms in the core shell and consequently larger contributions from the M^+–Ar interactions, which pushes up the binding energy as will be shown in Sec. VI B.

Table III shows the structures that result when the three-body term (from Sec. IV C) is included in the overall potential. The net effect of the ion–induced-dipole interaction is repulsive, but the details of its effect depend upon the cluster size. For instance, comparison of Tables II and III show that the dd potentials favor a linear M^+Ar_2 instead of a bent one, and tetrahedral core structures instead of octahedral ones (see $n = 6$–14 for I and II). It also appears that when the dd term is added to potential III the octahedral core becomes favored over those with square antiprism core. This is not the case for the much larger M^+ ion represented by the IV and IV + dd potentials; here the square antiprism (SAP) structure predominates for $n = 8$–14.

Additional understanding of the various structures can be gained by following our natural classification, based upon inner solvation shell, a little further. Table IV lists the three core geometries obtained with the eight potentials according to the size of their innermost solvation shell or core structure. The tetrahedral core seems to occur as a global minimum for very small metal ions. This is seen in the range of first-shell distances from the metal ion. The octahedral core is predicted for somewhat larger ions. The SAP core is found to have a large shell radius. Though these generalizations vary somewhat with addition of the repulsive dd term, it is clear that a larger ion allows more argon atoms in its innermost solvation shell.

B. Equilibrium binding energies

Table V gives the total binding energy $E_n = -\min(V_n)$ for each cluster. Plotting the various contributions to the total potential vs the number of argons n gives a better view of what is occurring as the clusters become larger. In Fig. 3 panels labeled I through IV and I + dd through IV + dd correspond to those total potentials. In panel I we see that the small Co^+ ion leads to a very compact tetrahedral core. As this core is capped the binding energy per argon drops dramatically. In panel I + dd we see basically the same behavior but the inclusion of the three-body term has lowered the total binding energy somewhat. This happens because the total dd term is always repulsive although individual terms in dd are attractive. Panel II shows the V^+ ion rapidly forming this tetrahedral core but then switching over to the higher coordination of the octahedral core at $n = 6$–10. The near isoenergetic structures of the tetrahedral

TABLE V. Binding energy (in eV) of $(M^+)Ar_n$ for potentials I to IV + dd.

n	I	II	III	IV	I + dd	II + dd	III + dd	IV + dd
	Binding energy in (eV) for potentials I to IV + dd							
1	0.524	0.381	0.403	0.299	0.524	0.381	0.403	0.299
2	1.060	0.774	0.818	0.610	0.936	0.699	0.790	0.589
3	1.537	1.165	1.245	0.932	1.166	0.919	1.157	0.871
4	1.903	1.511	1.678	1.259	1.292	1.073	1.505	1.144
5	2.001	1.612	2.092	1.596	1.347	1.129	1.785	1.405
6	2.099	1.773	2.517	1.946	1.401	1.167	2.063	1.659
7	2.195	1.841	2.583	2.161	1.454	1.240	2.114	1.793
8	2.292	1.913	2.717	2.276	1.517	1.290	2.166	1.925
9	2.375	1.984	2.801	2.473	1.581	1.303	2.217	1.987
10	2.458	2.059	2.885	2.560	1.632	1.418	2.278	2.035
11	2.543	2.149	2.944	2.614	1.697	1.480	2.341	2.096
12	2.627	2.234	3.013	2.675	1.788	1.565	2.394	2.152
13	2.658	2.301	3.072	2.742	1.829	1.615	2.446	2.209
14	2.765	2.402	3.140	2.814	1.889	1.667	2.509	2.259

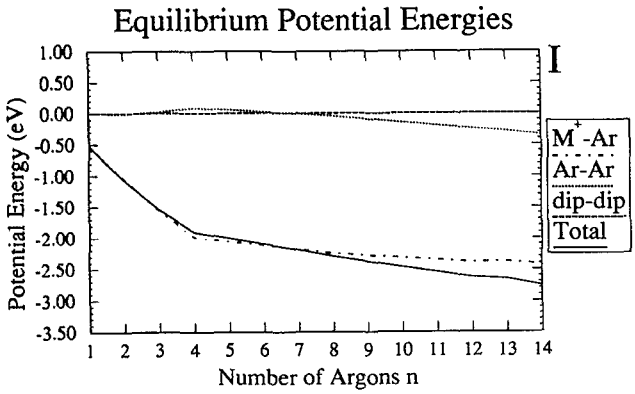

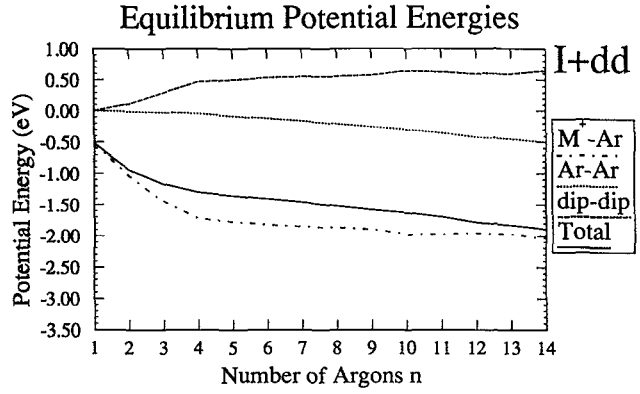

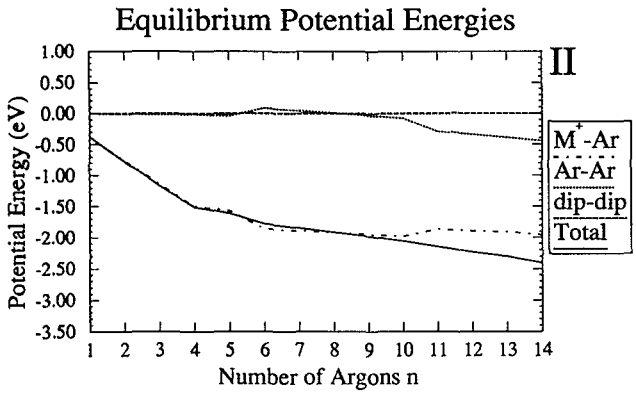

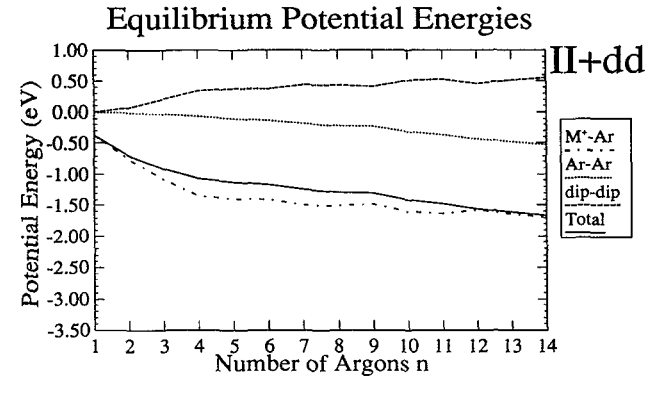

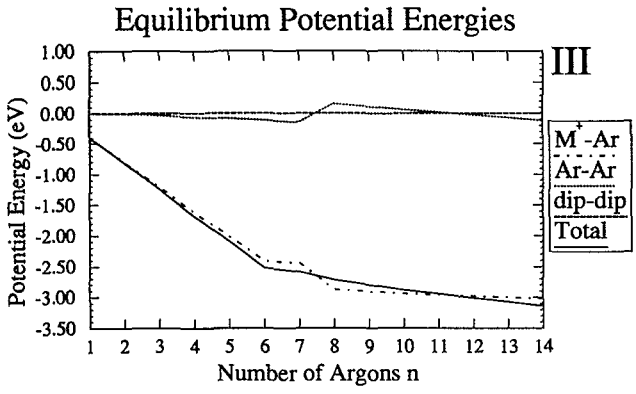

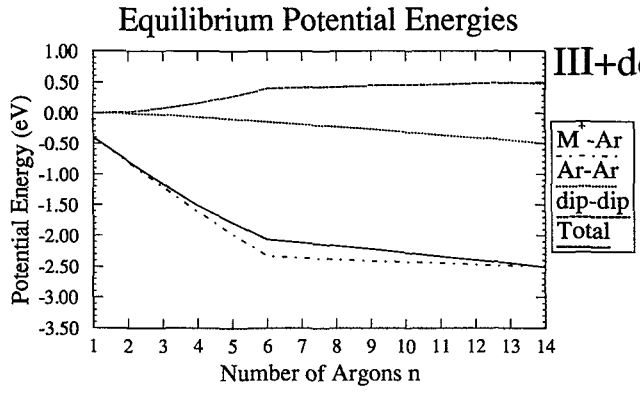

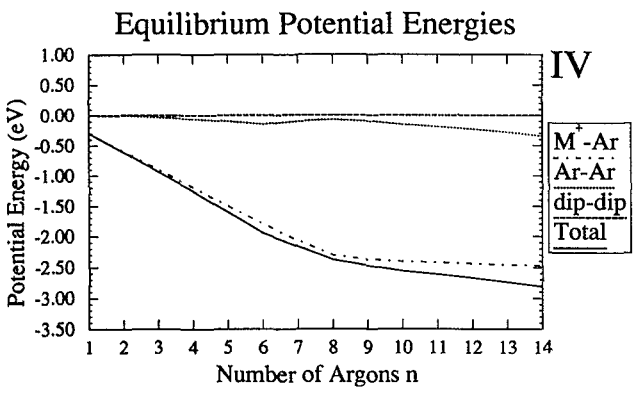

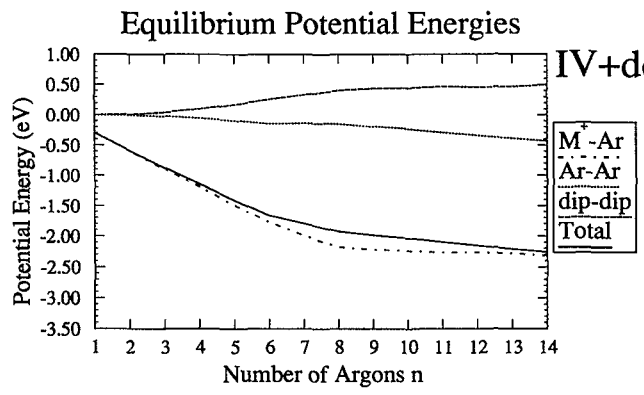

FIG. 3. Equilibrium potential-energy contributions to the total potential for I through IV + dd with M^+–Ar + Ar–Ar and M^+–Ar + Ar–Ar + dd terms. It is clear that the dd term always contributes as a repulsive term although some individual contributions from dd may be attractive. In general, the M^+–Ar potential dominates; however, as the M^+ becomes solvated the Ar–Ar interaction also becomes important.

core and octahedral core can be seen as n changes from 5 to 6 and again as n goes from 10 to 11. The tetrahedral core structures are formed for $n = 5$ and $n \geqslant 11$. It should be noted that the total potential decreases at a nearly constant rate although its contributions (namely, the M^+–Ar and Ar–Ar terms) have quite abrupt changes. Panel II + dd indicates that the tetrahedral core structures win out now with inclusion of the repulsion from the dd term. It should be noted that although a very symmetric $(V^+)Ar_{14}$ is possible, a less symmetric structure (egg shaped) is now favored. This is thought to occur because the repulsive energy from the induced dipoles of argons becomes comparable to the Ar–Ar interaction energy. This leads to an incomplete filling of the shell structures previously seen when the dd term was absent.

Panel III shows a monotonic decrease in potential until the octahedral structure is formed. This octahedral structure is then capped with one atom and then switches to a square antiprismatic core for $n = 8$–14. Comparison of panels III and III + dd shows that nearly isoenergetic structures are obtained with either an octahedral or square antiprismatic core. When the dd term is added, the repulsion energy pushes some of the SAP core atoms out and capping occurs on an octahedral core. Panel IV shows monatomic decrease in the potential energy to $n = 6$, but rather than capping the octahedron at $n = 7$ the cluster prefers a seven-coordinate structure. Then the SAP core structures take over for $n = 8$–14. Panel IV + dd shows the same behavior with slightly lower total binding energy due to the dd term. These plots give insight into which potential terms are important and also into where structural changes are taking place.

Figures 4(a) and 4(b) are plots of the adiabatic binding energy $\Delta E_n = E_n - E_{n-1}$ of the nth Ar atom for each of the potentials. Figure 4(a) shows results for potentials I to IV, i.e., without the dd interaction, while Fig. 4(b) shows results for I + dd to IV + dd. In Fig. 4(a) curve I indicates a large decrease in the binding energy for the fifth Ar added and leveling off in all contributions to the binding energy. This occurs because the fifth argon is further from the ion in a new solvation shell. This rapid leveling off of the adiabatic binding energy is seen, in general, after the formation of the first shell. In Fig. 4(b) curve I + dd has a similar appearance, except that the adiabatic binding energy falls more rapidly for the atoms of the first shell, due to the repulsion of the dd term. From Fig. 4(a), curve II, it is evident that while the adiabatic binding energy is leveling off after $n = 5$, the contributions to it are still fluctuating as the core changes from ctet to coct and back again. In Fig. 4(b) curve II + dd has small undulations, but for the most part it is approaching a constant value after $n = 5$. In Fig. 4(a), curve III, the break at $n = 6$ indicates the formation of an octahedral core. The jump at $n = 8$ is due to the formation of the SAP structure. In Fig. 4(b), curve III + dd, the core now forms instead at $n = 6$ and remains unchanged to $n = 14$. In Fig. 4(a), curve IV shows changes in the region where the switch from coct to csap occurs. The adiabatic binding energy in Fig. 4(b), curve IV + dd, levels off after formation of the SAP structure. A very appealing argument is that the larger clusters ($n > 8$ in most cases) are approaching bulk conformations.

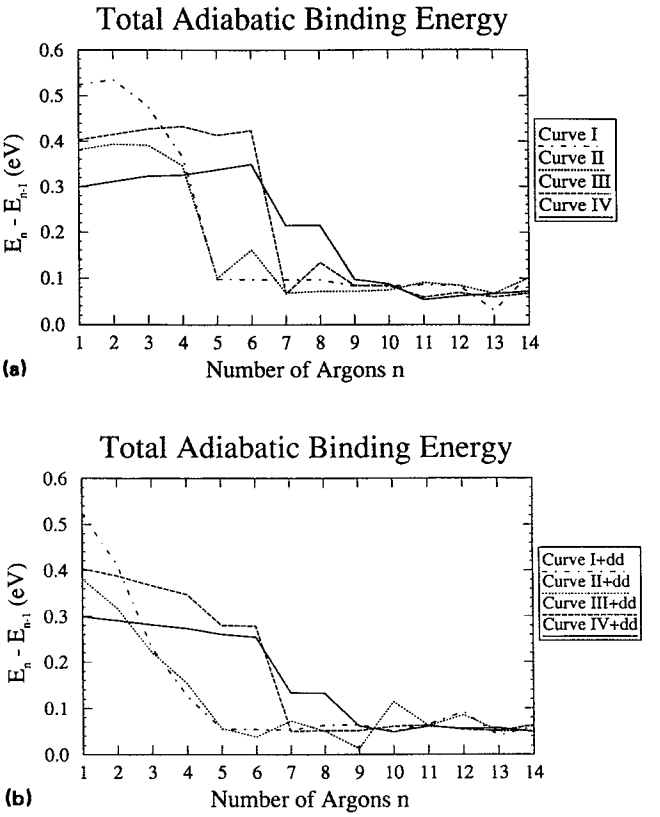

FIG. 4. Total adiabatic binding energy $\Delta E_n = E_n - E_{n-1}$ (with $E_0 = 0$) for all the parametrizations gives an idea of where shell closures occur. (a) refers to potentials without the dd interaction; (b) contains it. Comparing curves III and III + dd, it is clear that the shell closing occurred at $n = 6$, representing an octahedral core. Curve III, however, shows another break at $n = 8$ representing a new core structure, the square antiprism.

Figure 5 shows the contributions to ΔE_n from the two- and three-atom terms in the many-atom potential. This type of plot emphasizes the points of interest (such as structural changes and shell closures). The total Ar–Ar interaction is very near its bulk value of ca. 0.076 eV.[20] The (M^+)–Ar contribution also levels off rapidly and may be approaching its bulk value. However, we have found that the larger clusters are not approaching bulk values at the same rate for

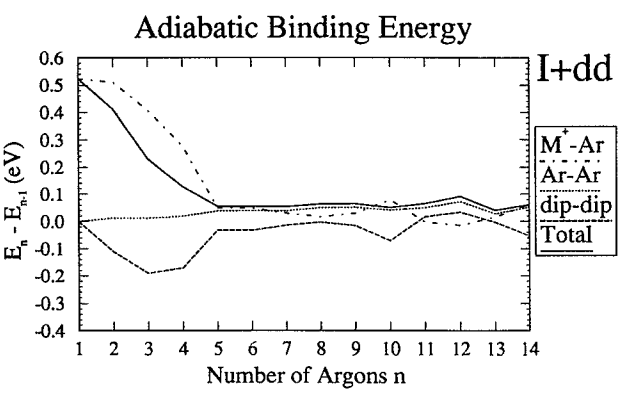

FIG. 5. Breakup of contributions to the adiabatic binding energy for I + dd, showing where the bulk limit for Ar–Ar and M^+–Ar is reached.

TABLE VI. Equilibrium rotational constants for I + dd and II + dd representing Co^+ and V^+, respectively.

	$(Co^+)Ar_n$ rotational constants (in $cm^{-1} \times 10^{-3}$)			$(V^+)Ar_n$ rotational constants (in $cm^{-1} \times 10^{-3}$)		
n	A	B	C	A	B	C
1	···	209	209	···	190	190
2	···	58	58	···	51	51
3	69	69	35	62	62	31
4	35	35	35	32	32	32
5	35	17	17	32	17	17
6	22	13	11	20	12	9.5
7	17	8.4	8.0	12	12	8.1
8	11	8.4	6.2	15	5.7	5.7
9	8.9	6.9	5.3	6.9	6.1	5.3
10	8.0	4.5	4.5	8.1	4.5	4.5
11	6.1	4.4	3.8	4.8	4.8	4.5
12	4.7	4.5	3.9	4.7	4.4	3.9
13	4.4	3.2	3.1	4.6	3.4	3.1
14	4.3	2.9	2.4	3.6	3.1	2.7

different size ions. Hence the rate at which cluster properties are approaching bulk values is governed not only by the strength of the interaction (D_e) but also by size of the ion (R_e).

C. Equilibrium properties

The equilibrium properties have been calculated from the $\beta \to \infty$ simulations. Reported here are the properties of the structures corresponding to potentials parametrized from experimental values, namely I and II, with the inclusion of the dd term. The moment of inertia tensor has been diagonalized via a rotation from the space-fixed frame to a body-fixed frame to obtain principal moments of inertia, and these have been inverted to give the rotational constants in cm^{-1}, listed in Table VI. These values are similar for the Co and V clusters, decreasing in general as n increases due to the larger moments of inertia. This table allows us to classify the clusters as spherical tops with $A = B = C$, as found for $(M^+)Ar_4$, prolate or oblate symmetric tops with $A = B \neq C$, and asymmetric tops, with $A \neq B \neq C \neq A$.

The COM dipoles and quadrupoles have been rotated into the same frame as the rotational constants and are reported in esu (10^{-18} esu = 1 D, so that water has a dipole of 1.84 D).

The COM dipole vector components and the vector magnitudes are listed in Table VII. Since the principal moments of inertia frame does not define the sign of the dipole, we have chosen the a-axis direction so as to give a positive D_a. Many of the small clusters (with $n = 2$–4) have small or zero dipole moments. The larger clusters have somewhat larger dipole moments due to their lower symmetry and the displacement of the charge from the center of mass. The symmetry of many of the larger clusters is shown by a single nonzero dipole vector component.

The COM quadrupole-tensor components are given in Table VIII for the I + dd and II + dd structures. The highly

TABLE VII. Equilibrium COM electric dipole moment vector components and magnitudes for I + dd and II + dd representing Co^+ and V^+, respectively, in the principal moments of inertia frame, with the a-axis direction chosen to give a positive D_a.

	$(Co^+)Ar_n$ COM dipole moments (in 10^{-18} esu)				$(V^+)Ar_n$ COM dipole moments (in 10^{-18} esu)			
n	D_a	D_b	D_c	D	D_a	D_b	D_c	D
1	1.21	0.00	0.00	1.21	2.18	0.00	0.00	2.18
2	0.00	0.00	0.00	0.00	0.00	0.00	0.00	0.00
3	0.00	0.00	0.00	0.00	0.00	0.00	0.00	0.00
4	0.00	0.00	0.00	0.00	0.00	0.00	0.00	0.00
5	2.31	0.00	0.00	2.31	2.33	0.00	0.00	2.33
6	0.00	2.24	0.00	2.24	0.03	2.81	0.10	2.81
7	1.81	−1.72	−1.46	2.89	0.00	0.00	1.66	1.66
8	5.16	−2.01	0.38	5.55	0.00	1.71	0.00	1.71
9	4.46	−3.49	−0.32	5.67	2.29	1.46	−2.50	3.68
10	0.00	0.00	0.00	0.00	0.00	0.00	0.00	0.00
11	2.90	−1.67	−2.51	4.19	0.00	0.00	2.46	2.46
12	7.01	0.06	1.47	7.16	7.32	0.04	−1.55	7.48
13	0.31	−3.70	5.16	6.36	3.33	−0.01	−3.78	5.03
14	3.39	−0.30	2.44	4.19	1.54	3.43	0.17	3.76

TABLE VIII. Equilibrium COM electric quadrupole tensor components and magnitudes for I + dd and II + dd representing Co^+ and V^+, respectively. The value of Q_{cc} follows from $Q_{aa} + Q_{bb} + Q_{cc} = 0$.

	$(Co^+)Ar_n$ quadrupole moments (in 10^{-26} esu)					$(V^+)Ar_n$ quadrupole moments (in 10^{-26} esu)				
n	Q_{aa}	Q_{ab}	Q_{ac}	Q_{bb}	Q_{bc}	Q_{aa}	Q_{ab}	Q_{ac}	Q_{bb}	Q_{bc}
1	15.64	0.00	0.00	−7.82	0.00	16.33	0.00	0.00	−8.16	0.00
2	33.59	0.00	0.00	−16.79	0.00	31.30	0.00	0.00	−15.65	0.00
3	11.90	0.00	0.00	11.90	0.00	11.25	0.00	0.00	11.25	0.00
4	0.00	0.00	0.00	0.00	0.00	0.00	0.00	0.00	0.00	0.00
5	10.06	0.00	0.00	−5.03	0.00	9.84	0.00	0.00	−4.92	0.00
6	7.00	0.00	0.00	1.91	0.00	8.89	−0.44	1.17	1.62	−0.20
7	11.76	−3.44	−0.71	−3.94	2.81	3.37	0.00	0.00	3.37	0.00
8	19.45	−8.35	4.49	−1.87	−0.24	16.28	0.00	2.42	−6.12	0.00
9	15.38	−11.78	1.77	3.82	1.05	7.44	4.17	−4.23	−1.88	−3.37
10	14.87	0.00	0.00	−7.44	0.00	14.51	0.00	0.00	−7.25	0.00
11	11.42	−3.97	−7.46	−0.90	4.82	−1.06	0.00	0.00	−1.06	0.00
12	28.14	0.33	11.66	−9.61	0.10	29.65	0.20	−12.38	−10.53	−0.06
13	−2.15	−4.43	1.83	−4.60	−19.88	11.91	−0.10	−7.22	−8.68	0.03
14	21.15	0.55	10.12	−5.19	−0.18	5.94	3.76	1.61	5.10	0.28

symmetric clusters have small off-diagonal tensor components, as expected in the body-fixed (or principal moments of inertia) frame.

VII. DISCUSSION AND CONCLUSION

Several qualitative conclusions can be reached by considering the effects of changing potentials for each cluster type. The experimentally determined $(M^+)Ar$ interaction potentials give a strongly bound and compact inner solvation shell structure for each cluster, with deeper wells and small equilibrium distances. The parametrized theoretical potentials tend to yield clusters with a less-compact inner solvation shell, and contain more argons with higher total binding energy.

It has been observed that the outer region of the $(M^+)Ar$ potential is very important. Shifting its location can affect the size of the first solvation shell and therefore the number of strong interactions. Also, it has been shown that the repulsive interaction of charge-induced dipoles can yield a large effect on these solvation shells. In fact, the dd term may be overestimating the repulsion. Other terms in the multipole expansion might eliminate the egg-shaped clusters found for $n = 10$–14. These egg-shaped clusters are reminiscent of the results observed by Barnett, Landman, and Cleveland for electrons bound to $(NH_3)_n$ and $(H_2O)_n$. Their quantal calculations yield surface states in which a localized electron density, which starts around the COM, eventually moves almost entirely to the outside of the cluster.[21] In our classical calculations, the ion is moving out from the COM to form an egg-shaped cluster so as to increase the binding among induced dipoles which align once the M^+–Ar attraction has dropped sufficiently.

The method of simulated annealing is very effective for finding the global minimum on a complicated potential-energy surface. However, for the larger clusters this global minimum is nearly isoenergetic with many of the local minima; therefore, computer time for simulated annealing increases rapidly with n. These isoenergetic minima are undoubtedly within accessible phase space at finite temperatures. Further understanding about the solvation effects associated with these PESs would result from classical dynamics modeling such as has been done for the Ar_n systems treated by Wales and Berry.[7]

In our study, we verified that we had reached the global minimum of a cluster, instead of some local minima or other stationary point, by repeating the SA procedure for each cluster with different initial conditions. An alternative way of verifying we had minima, more definitive but very time-consuming for our many potentials and clusters, would have been to calculate force constants at our equilibrium conformations. This would also allow for normal-mode analysis. Instead of proceeding this way, we are exploring alternative ways to obtain vibrational frequencies directly from dynamical properties of the clusters.[22]

We hope to apply these types of approaches to more complicated clusters. Most interesting will be the application to $(V^+)(H_2O)_n$ and $(V^+)(CO_2)_n$, since the $(V^+)(H_2O)$ and $(V^+)(CO_2)$ photodissociation spectra are currently being experimentally investigated.[23,24] The potentials selected with the SA technique can be used in future work to also include the classical molecular-dynamics modeling of these and similar clusters.

ACKNOWLEDGMENTS

This work has been partly supported by NSF Grants No. CHE-8615334 and No. CHE-8918925, and by Florida Space Consortium Grants NASA No. NGT-40015 and University of Florida No. DSR U001.

[1] D. A. Micha, J. Mol. Struct. **199**, 225 (1989).
[2] M. A. Johnson and W. C. Lineberger, in *Techniques for the Study of Ion Molecules Reactions*, edited by J. M. Farrar and W. Saunders (Wiley, New York, 1988), p. 591.
[3] E. E. Ferguson, Annu. Rev. Phys. Chem. **26**, 17 (1975).

[4] J. M. Parson, P. E. Siska, and Y. T. Lee, J. Chem. Phys. **56**, 1511 (1972).
[5] D. Lessen and P. J. Brucat, J. Chem. Phys. **90**, 6296 (1989); **91**, 4522 (1989).
[6] D. E. Lessen, R. L. Asher, and P. J. Brucat, Int. J. Mass Spectrosc. Ion Proc. **102**, 331 (1990).
[7] D. J. Wales and R. S. Berry, J. Chem. Phys. **92**, 4283 (1990); D. J. Wales, J. Am. Chem. Soc. **112**, 7908 (1990).
[8] J. Leech, Math. Gazette **41**, 81 (1957).
[9] L. T. Wille, Chem. Phys. Lett. **133**, 405 (1987).
[10] I. M. Navon, F. B. Brown, and D. H. Robertson, Comput. Chem. (in press).
[11] E. T. Jaynes, Annu. Rev. Phys. Chem. **31**, 579 (1980).
[12] J. B. Marion, *Classical Dynamics of Particles and Systems* (Academic, New York, 1970).
[13] J. O. Hirschfelder, C. F. Curtiss, and R. B. Bird, *Molecular Theory of Gasses and Liquids* (Wiley, New York, 1954).
[14] J. I. Steinfeld, *Molecules and Radiation* (MIT, Cambridge, MA, 1974), p. 214.
[15] C. W. Bauschlicher, Jr., H. Partridge, and S. R. Langhoff, J. Chem. Phys. **91**, 4733 (1989).
[16] P. W. Atkins, *Physical Chemistry* (Freeman, New York, 1986), p. 829.
[17] S. Kirkpatrick, C. D. Gelatt, and M. P. Vecchi, Science **220**, 671 (1983).
[18] D. Vanderbilt and S. G. Louie, J. Comput. Phys. **56**, 259 (1984).
[19] N. Metropolis, A. Rosenbluth, M. Rosenbluth, A. Teller, and E. Teller, J. Chem. Phys. **21**, 1087 (1953).
[20] *American Institute of Physics Handbook*, edited by D. E. Gray (McGraw-Hill, New York, 1957).
[21] R. N. Barnett, Uzi Landman, and C. L. Cleveland, J. Chem. Phys. **88**, 4429 (1988).
[22] R. L. Asher, P. J. Brucat, and D. A. Micha (unpublished).
[23] D. E. Lessen, R. L. Asher, and P. J. Brucat, J. Chem. Phys. **93**, 6102 (1990).
[24] D. E. Lessen, R. L. Asher, and P. J. Brucat, J. Chem. Phys. **95**, 1414 (1991).